European Journal of Pharmacology 907 (2021) 174297

Contents lists available at ScienceDirect

European Journal of Pharmacology

journal homepage: www.elsevier.com/locate/ejphar

XHL11, a novel selective EGFR inhibitor, overcomes EGFR^{T790M}-mediated resistance in non-small cell lung cancer

Yi Li [1], Qing-Long Yu [1], Tong-Fang Li, Ya-Ni Xiao, Li Zhang, Qiu-Yan Zhang [**], Chun-Guang Ren [***], Hong-Lei Xie [*]

Yantai Key Laboratory of Nanomedicine & Advanced Preparations, Yantai Institute of Materia Medica, Shandong, 264000, China

ARTICLE INFO

Keywords:
Non-small cell lung cancer
EGFR^{T790M}
EGFR TKI
Apoptosis

ABSTRACT

The first-generation epidermal growth factor receptor (EGFR) tyrosine kinase inhibitors (TKIs), gefitinib and erlotinib significantly improved the therapeutic effect in non–small cell lung cancer (NSCLC) patients with EGFR mutation. However, the EGFR^{T790M} mutation occurs and results in acquired resistance. Consequently, mutant selective third-generation EGFR TKIs represented by AZD9291 (Osimertinib) have been developed to offer more effective therapeutic treatment, but the clinical application is limited by the acquired resistance and the high costs. A series of 5-chloropyrimidine-2,4-diamine derivatives were synthesized and screened for *in vitro* anti-tumor activity on H1975 and A431 cells. XHL11 showed the strongest antineoplastic activity. Compared to AZD9291, XHL11 suppressed cellular proliferation and colony formation and induced apoptosis in H1975 cells with EGFR$^{L858R/T790M}$ mutation. In addition, XHL11 caused expression changes in EGFR and apoptosis-related pathways. Moreover, oral administration of XHL11 suppressed tumor progression *in vivo* in a H1975 subcutaneous xenograft model. These data demonstrated that XHL11 might be developed as a promising EGFR TKI for the therapeutic use of NSCLC patients.

1. Introduction

Lung cancer is the most commonly diagnosed cancer (11.6% of the total cases) and also the most frequent cause of cancerous mortality worldwide. It accounts for 18.4% of all the cancer-related deaths (Bray et al., 2018). EGFR mutations have been detected in the majority of NSCLC patients and accelerate the progression of the disease (Engelman and Janne, 2008; Heigener and Reck, 2011). Abnormal activation of EGFR resulted in dysregulation of the downstream pathways, such as MAPK and JNK pathways (Engelman and Janne, 2008; Tan et al., 2016), and contributed to the fatality rate.

EGFR has been reported to be one of the most successful targets for NSCLC (Rosell et al., 2009). Patients with EGFR gene mutations, such as the exon 19 deletion and L858R mutation, are sensitive to EGFR TKIs (Camidge et al., 2014; Park et al., 2016). The first and the second generations EGFR TKIs, such as gefitinib, erlotinib and afatinib, regulated EGFR pathways (Sequist et al., 2013) and participated in combination therapy. Unfortunately, the majority of patients eventually develop acquired resistance after about 1 year of treatment (Kobayashi et al., 2005). A secondary mutation in exon 20 (T790M) improved the ATP-binding capacity of the mutated protein and induced the resistance in approximately 60% of these resistant cases (Pao et al., 2005). Therefore, there remains an urgent requirement for an EGFR TKI which could overcome T790M-mediated resistance.

The third generation EGFR TKIs, such as WZ4002 (Zhou et al., 2009), CO-1686 (Walter et al., 2013) and AZD9291 (Janne et al., 2015) were developed to overcome the EGFR^{T790M}-mediated resistance and reduce the unwanted side effects. AZD9291 which was approved by the FDA performed the best, and improved the progression-free survival of NSCLC patients with T790M mutation (Goss et al., 2016; Yu et al., 2020). AZD9291 was reported to inhibit the phosphorylation of EGFR *in vitro*, resulting in the suppression of EGFR downstream signal pathways including Akt and ERK (Ku et al., 2016). However, the third-generation EGFR TKI also developed new acquired resistance after an average of 9.6

* Corresponding author
** Corresponding author
*** Corresponding author
E-mail addresses: qyzhang@yimm.ac.cn (Q.-Y. Zhang), cgren@yimm.ac.cn (C.-G. Ren), qingteng51@163.com (H.-L. Xie).
[1] These authors contribute equally.

https://doi.org/10.1016/j.ejphar.2021.174297
Received 1 February 2021; Received in revised form 23 June 2021; Accepted 28 June 2021
Available online 2 July 2021

months of treatment (Murtuza et al., 2019). The primary cause of acquired resistance to third-generation EGFR TKIs was $EGFR^{C797S}$ mutation (Niederst et al., 2015), along with ERBB2 and MET amplifications KRAS mutations (Ortiz-Cuaran et al., 2016) as possible mechanisms. The C797S mutation influences the covalent binding of AZD9291 and EGFR by changing the cysteine sidechain. The acquired resistance together with the high price and several adverse reactions limited the prescription of AZD9291. Therefore, further exploration and research are needed to find more safe, effective and economical agents to overcome therapeutic resistances caused by $EGFR^{C797S}$ mutation in lung cancer.

In this study, a series of 5-chloropyrimidine-2,4-diamine derivatives were synthesized and identified as potent EGFR inhibitors. We discovered a novel selective EGFR TKI, XHL11, which effectively inhibited the $EGFR^{L858R/T790M}$ and $EGFR^{L858R/T790M/C797S}$ kinases activity. Molecular docking of the new compounds into the EGFR was also performed. The down-regulation of EGFR and the down-stream pathways by XHL11 contributed to the apoptosis and the regulation of cellular proliferation in H1975 cells with $EGFR^{L858R/T790M}$ mutation. These results suggested that XHL11 might be developed as a promising EGFR TKI for the treatment of NSCLC patients.

2. Materials and methods

2.1. Chemistry

5-chloro-N^4-(2-(isopropylsulfonyl)phenyl)-N^2-(3-nitrophenyl)pyrimidine-2,4-diamine: A mixture of 2,5-dichloro-*N*-(2-(isopropylsulfonyl)phenyl)pyrimidin-4-amine (3.5 g, 10 mmol), 3-nitroaniline (1.6 g, 12 mmol) and isopropyl alcohol 40 ml were added to a 250 m three-necked round bottom flask. The solution was heated to 85 °C for 8 h and then cooled to room temperature. The precipitate was filtered, washed with water, and then purified by column chromatography (silica gel) to give target product (3.5 g, 79.5% yield) as a yellow solid. ESI-MS: m/z = 447.89 [M + H].

N^2-(3-aminophenyl)-5-chloro-N^4-(2-(isopropylsulfonyl)phenyl)pyrimidine-2,4-diamine:5-chloro-N^4-(2-(isopropylsulfonyl)phenyl)-N^2-(3-nitrophenyl)pyrimidine-2,4-diamine (3.0 g, 6.7 mmol) was dissolved in methanol 60 ml, Pd/C 0.3 g was added, and then reaction with H_2. The reaction mixture was stirred at room temperature for 6 h. The Pd/C was filtered, washed with methanol, the filtrate was dried and obtained product (2.6 g, 92.8% yield) as a yellow solid. ESI-MS: m/z = 417.91 [M + H].

Compound XHL 11:

A mixture of N^2-(3-aminophenyl)-5-chloro-N^4-(2-(isopropylsulfonyl)phenyl)pyrimidi-ne-2,4-diamine (2.4 g, 5.7 mmol), acryloyl chloride (0.5 g, 6.2 mmol) and dichloromethane 20 ml were added to a 100 ml three-necked round bottom flask. The reaction mixture was stirred at room temperature for 2 h, and then dried and purified by column chromatography (silica gel) to give target product (2.0 g, 75% yield) as a light white solid. ESI-MS: m/z = 471.11 [M + H]. ^{1}H NMR (400 MHz, DMSO-d_6): δ (ppm):

1.17 (s, 3H), 1.18 (s, 3H), 3.43–3.47 (m, *J* = 2 Hz, 1H), 5.73–5.72 (d, *J* = 2 Hz, 1H), 5.76–5.75 (d, *J* = 2 Hz, 1H), 6.46–6.25 (t, *J* = 3 Hz, 1H), 7.22–7.20 (d, *J* = 2 Hz, 1H), 7.35–7.33 (m, *J* = 0.5 Hz, 3H), 7.81 (d, *J* = 0.2 Hz, 1H), 7.82 (d, *J* = 0.2 Hz, 1H), 7.94 (s, 1H), 8.30 (s, 1H), 8.70–8.68 (d, *J* = 2 Hz, 1H), 9.55 (s, 1H), 9.59 (s, 1H), 10.07 (s, 1H). ^{13}C NMR (101 MHz, DMSO-d_6): δ (ppm): 15.34, 55.46, 105.51, 111.94, 114.17, 116.01, 123.98, 124.16, 124.55, 127.23, 129.10, 131.43, 132.50, 135.37, 138.53, 139.62, 140.82, 155.30, 155.69, 158.22, 163.56.

HPLC purity 98.67% (0–3 min, A: 30% methanol (0.1% trifluoroacetic acid), B:70% water (0.1% trifluoroacetic acid); 4–15 min, A: 95% methanol (0.1% trifluoroacetic acid), B:5% water (0.1% trifluoroacetic acid); 16–18 min, A: 30% methanol (0.1% trifluoroacetic acid), B:70% water (0.1% trifluoroacetic acid) (Fig. S1A).

Compound XHL 11a: *N*-(4-((5-chloro-4-((2-(isopropylsulfonyl)phenyl)amino)pyrimidin-2-yl)amino)phenyl)acrylamide was obtained as a light white solid. Yield: 77%. Purity 99.53% (Fig. S1B), ESI-MS: m/z = 471.11 [M + H]. ^{1}H NMR (400 MHz, DMSO-d_6): δ (ppm): 1.16 (s, 3H), 1.17 (s, 3H), 3.48–3.45 (m, *J* = 2 Hz, 1H), 5.72–5.71 (d, *J* = 2 Hz, 1H), 5.74–5.73 (d, *J* = 2 Hz, 1H), 6.26–6.25 (t, *J* = 1.6 Hz, 1H), 7.38 (d, *J* = 0.2 Hz, 1H), 7.42–7.40 (m, *J* = 1 Hz, 4H), 7.74 (m, *J* = 0.2 Hz, 1H), 7.85–7.84 (d, *J* = 2 Hz, 1H), 7.87–7.86 (m, *J* = 2 Hz,1H), 8.18 (s, 1H), 8.28 (s, 1H), 9.46 (s, 1H), 9.52 (s, 1H), 10.05 (s, 1H). ^{13}C NMR (101 MHz, DMSO-d_6): δ (ppm): 15.39, 55.38, 100.00, 105.02, 114.34, 120.15, 120.54, 124.23, 126.91, 131.47, 132.52, 133.95, 135.31, 136.26, 138.56, 155.43, 155.80, 158.18, 163.28.

Compound XHL 11 b: *N*-(3-((5-chloro-4-((2-(isopropylsulfonyl)phenyl)amino)pyrimidin-2-yl)amino)phenyl)-2-cyanoacetamide was obtained as a light white solid. Yield: 82%. Purity 99.19% (Fig. S1C), ESI-MS: m/z = 484.11 [M + H]. ^{1}H NMR (400 MHz, DMSO-d_6): δ (ppm): 1.17 (s, 3H), 1.19 (s, 3H), 3.47–3.44 (t, *J* = 4 Hz, 1H), 3.87 (s, 2H), 7.17–7.16 (d, *J* = 1.3 Hz, 1H), 7.20–7.18 (d, *J* = 4 Hz, 1H), 7.38–7.37 (m, *J* = 2 Hz, 2H), 7.73–7.71 (d, *J* = 4 Hz, 1H), 7.85–7.83 (d, *J* = 4 Hz, 2H), 8.30 (s, 1H), 8.67–8.64 (d, *J* = 6 Hz, 1H), 9.54 (s, 1H), 9.62 (s, 1H), 10.23 (s, 1H). ^{13}C NMR (101 MHz, DMSO-d_6): δ (ppm): 15.40, 27.23, 55.47, 105.61, 111.50, 113.78, 116.11, 116.48, 124.06, 124.24, 129.23, 131.48, 135.40, 138.50, 138.98, 140.99, 144.36, 155.31, 155.63, 158.06, 161.32.

2.2. Biology

2.2.1. Reagents

AZD9291 was purchased from MedChemExpress (MCE, NJ, USA), Gefitinib was purchased from J&K Scientific Ltd (Beijing, China), MTT was obtained from Sigma-Aldrich (St. Louis, MO, USA). The primary antibodies against EGFR, phosphor-EGFR, ERK, phosphor-ERK, PARP were purchased from Cell Signaling Technology (Danvers, MA, USA); antibodies against Ki67 were purchased from Santa Cruz Biotechnology (Santa Cruz, CA, USA). The Annexin V-FITC Assay kit, Reactive Oxygen Assay Kit, Crystal Violet Staining Solution and N-Acetylcysteine (NAC) were purchased from Beyotime Institute of Biotechnology (Shanghai, China).

2.2.2. Molecular docking

Crystal structure of EGFR (PDB ID: 6LUB) and inhibitors were both pretreated by Discovery Studio 3.5. All docking runs were utilizing LigandFit Dock protocol of Discovery Studio 3.5. The image files are generated by the Accelrys DS visualizer 4.0 systems.

2.2.3. Cell culture

Human NSCLC cell lines H1975 and A431 were obtained from American Type Culture Collection (Manassas, VA), which were cultured in RPMI1640 medium (Gibco, Grand Island, NY, USA). PC9 cell line were purchased from Jiangsu Meimian industrial Co., Ltd (Jiangsu, China), which were cultured in DMEM medium (Gibco, Grand Island, NY, USA). All cultured mediums were supplemented with 10% fetal bovine serum (FBS, Gibco) and 1% solution of antibiotics (Hyclone, Logan, UT, USA) at 37 °C in an incubator with 5% CO_2.

2.2.4. Kinase enzymatic activity assay

The Z′-Lyte Kinase Assay Kit, WT and mutated EGFR kinase enzyme were purchased from Invitrogen. Kinase enzymatic activity assay was performed in accordance with the instructions of the manufacturer. In brief, prepare test compounds at four times the expected concentrations in the 10 μl Kinase Reactions. The compound, ATP solution and kinase/peptide mixture were mixed and incubated at the room temperature for 1 h. After the mixture of the development solution, the assay plate was incubated at room temperature for 1 h. At last, stop reagent was added to the plate. The activity was measured with a microplate reader (Molecular Devices).

2.2.5. Cell survival assay

H1975 and A431 cells were incubated with various concentrations of EGFR TKIs for 24, 48, 72 h. Tetrazolium dye (MTT) solution (5 mg/ml) was added to each well. After at last 4 h incubation, 100 μl dimethyl sulfoxide (DMSO) was added to each well to dissolve the formazan crystals. The absorbance was read at a test wavelength of 570 nm with a microplate reader (Molecular Devices). The IC_{50} values were calculated using the SPSS software (SPSS Inc., Chicago, IL, USA).

2.2.6. Colony formation assay

H1975 and A431 cells were seeded into 6-well plates at a density of 200–300 cells per well. The medium was replaced by fresh media containing different concentrations of XHL11. After incubated with series concentration of XHL11 for 48 h, the cells were cultured with fresh media for 10 d, and fixed by 4% paraformaldehyde. After being washed by PBS, the cells were stained with Crystal Violet Staining Solution. The colonies (≥50 cells) were counted and the typical images were photographed.

2.2.7. Flow cytometry analysis

Annexin V-FITC apoptosis analysis was performed using the Annexin V-FITC apoptosis detection kit. Briefly, cells were seeded into the 6-well plate overnight, and treated with Gefitinib, AZD9291 and XHL11 for 24 h. Cells were harvested using trypsinization, washed by PBS, and re-suspended in 500 μl buffer together with 5 μl of Annexin V-FITC and 5 μl of PI, and incubated for 30 min at room temperature, and analyzed by a flow cytometer (BD Accuri C6, Franklin Lakes, NJ).

2.2.8. Western blot analysis

About 5×10^6 H1975 cells were gathered after incubated with XHL11 for 24 h and lysed with RIPA buffer together with protease inhibitor (PMSF) and phosphatase inhibitor (NaF). Equal amounts of protein extracted from H1975 cells were electrophoresed by 8–10% SDS-PAGE and transferred onto polyvinylidene difluoride (PVDF) membranes. After blocked with milk for 1 h at room temperature, the membranes were incubated with primary antibodies and horseradish peroxidase (HRP)-conjugated secondary antibodies, and the reacted with ECL detection reagents (Thermo Scientific). The immune reactive bands were visualized in Amersham Imager 680 (GE Healthcare, Buckinghamshire, UK).

2.2.9. Detection of intracellular reactive oxidative species production

H1975 and A431 cells were seeded into the 6-well plate overnight, and treated with indicated compounds for 24 h, and Rosup compound mixture for 30 min. The Rosup group was incubated with Rosup compound mixture, which could activate the reactive oxidative species generation within 30 min. After incubation for 30 min with diluted DCFH-DA (10 μM), the cells were washed with PBS and photographed by microscopy (Ti–U, Nikon). Data were expressed as % of control.

2.2.10. Subcutaneous xenografts studies

Male nude mice were obtained from Gem Pharmatech Co., Ltd and raised on a 12-h light-dark cycle. The animal experiment were approved by the Committee on the Ethics of Animal Experiments of the Yantai Institute of Materia Medica, and were performed in strict accordance with the relevant institutional and national guidelines and regulations. The ethical approval number is 20191011-1. Briefly, H1975 cells (2×10^6 cells/200 μl) were subcutaneously injected to the left flank of mice. Mice were randomized into two groups (n = 5), when the average tumor volume reached 100 mm^3. It was reported that the antitumor efficacy in xenograft mouse models of H1975 for the novel selective EGFR inhibitors against $EGFR^{L858R/T790M}$ resistance mutation was evaluated at 100 mg/kg once daily or 50 mg/kg twice daily orally (Hao et al., 2016). Considering the oral absorption rate and first pass effect, the mice in the treatment group were treated with XHL11 (60 mg/kg) twice a week by oral gavage for 17 days. The mice in vehicle control group were intragastric administrated with 5% carboxymethyl cellulose sodium (CMC-Na) twice a week. Tumor volume was measured three times a week with a caliper (calculated volume = shortest diameter^2 × longest diameter/2). After 17 days treatment, tumor-bearing mice were euthanized and tumor tissues were removed for immunohistochemistry staining.

2.2.11. Immunohistochemistry staining

Tumor samples were fixed in 10% formalin at room temperature and paraffin embedded. Tumor sections were then deparaffinized and antigen retrieval. After blocking for half an hour at room temperature, the sections were incubated with the primary antibody overnight at 4°C. After washing three times with PBS, sections were then treated with anti-rabbit secondary antibody for 1 h at room temperature, and then developed by DAB reagent for 1 min. Some of the tumor sections were subjected to TUNEL assay according to the manufacturer's protocol (Beyotime Institute of Biotechnology). Positive nuclei were stained with brown colour. Images were taken by a Nikon Ti–U fluorescent microscope with a CCD digital camera (magnification, × 200). Staining intensity was scored as 0 (negative), 1 (weak), 2 (medium) and 3 (strong). Extent of staining was scored as 0 (0%), 1 (1–25%), 2 (26–50%), 3 (51–75%) and 4 (76–100%), according to the percentage of the whole carcinoma area which was positively stained. The product of the intensity score and the extent score was expressed as the staining score.

2.2.12. Statistical analysis

All the data are expressed as mean values ± standard deviation (S.D.). Comparisons among multiple groups were made with a one-way analysis of variance (ANOVA) followed by Dunnett's test using SPSS 13.0 software and GraphPad Prism 6. $P < 0.05$ was used for statistical significance.

3. Results

3.1. XHL11 was screened out as a novel mutant selective EGFR TKI

On the basis of AZD9291 functional group, we retained the 2,4,5-substituted pyrimidine core, and chose preponderant EGFR TKI inhibition drug fragments reported in literature as substituents for 4-substituted pyrimidine. The target EGFR TKIs were synthesized as shown in Scheme 1 and evaluated for their antiproliferative activity in H1975 cells with $EGFR^{L858R/T790M}$ mutation and in A431 cells with EGFR high expression. As shown in Table 1, XHL11 showed the highest antineoplastic activity with the IC_{50} of 0.055 ± 0.030 μM in H1975 cells, and 0.034 ± 0.04 μM in A431 cells after 48 h treatment. Therefore, we choose XHL11 for further research.

To further elucidate the binding pattern observed, molecular docking of the most potent inhibitor XHL11 were performed in the binding site cavity of EGFR. The binding modes of compound XHL11 and EGFR were depicted in Fig. 1B, which revealed that the inhibitor is well occupied in the binding pocket. As shown in Fig.1B, N-1 and 2-amino on the pyrimidine and Met-393 contribute to the hydrogen bonding interaction together, being a probable explanation for its activity. One hydrophobic interaction is formed between the 3-aniline and Pro 794. The 5-chloride on the pyrimidine and Thr864 contribute to the covalent bonding interaction.

3.2. XHL11 inhibited the EGFR kinase activity and the activation of EGFR

$EGFR^{C797S}$ mutation has been recently reported to contribute the most to the AZD9291 acquired resistance in patients with relapse (Thress et al., 2015). At the same time, the $EGFR^{C797S}$ mutation in a majority of AZD9291-resistant patients shed light on the development of novel EGFR inhibitors. The research and development of novel molecules and strategies to overcome $EGFR^{C797S}$ mutation are urgently warranted. As shown in Table 2, XHL11 was demonstrated to inhibit the

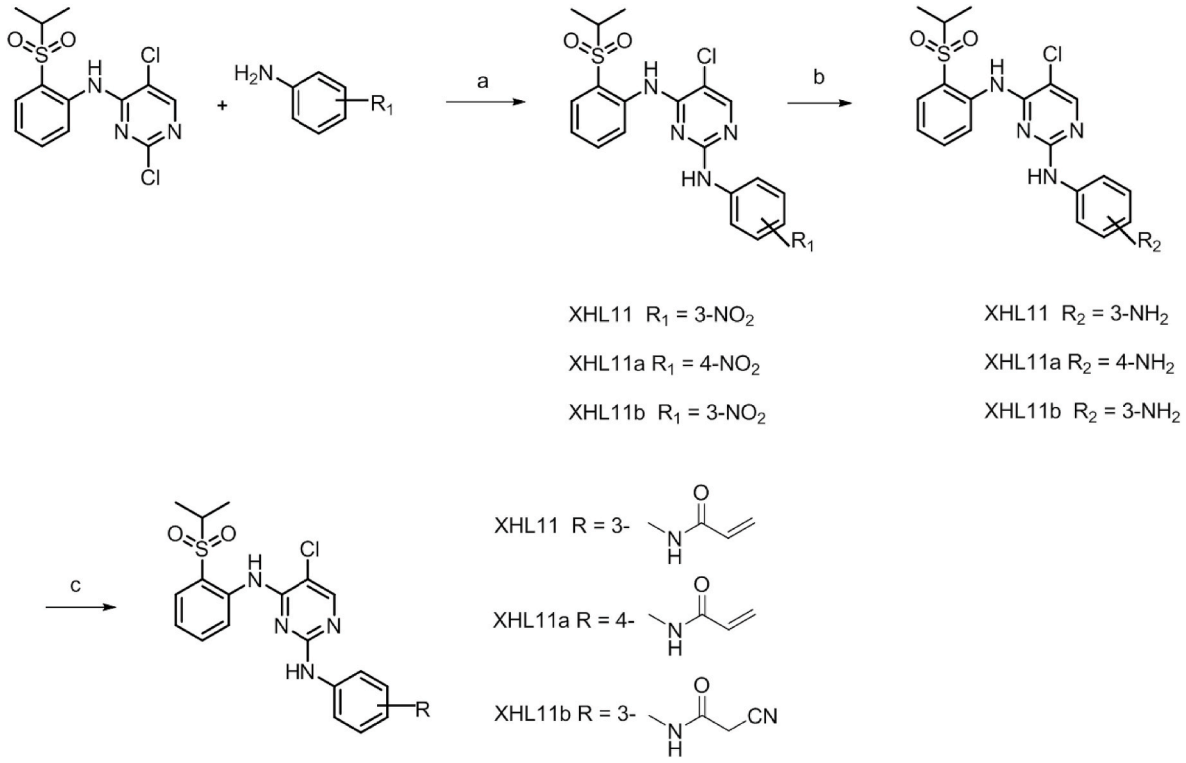

Scheme 1. Synthetic routes. Reagents and conditions: a) isopropyl alcohol, 85°C; b) Pd/C, MeOH, RT; c) DCM, RT.

Table 1
Antiproliferative activity of target compounds.

Compound	IC_{50}(μM)	
	H1975	A431
XHL11	0.055 ± 0.030	0.034 ± 0.04
XHL11a	0.081 ± 0.024	0.037 ± 0.024
XHL11b	0.40 ± 0.18	0.29 ± 0.08
AZD9291	0.18 ± 0.02	1.29 ± 0.32

IC_{50} values = mean ± SD of three independent assays.

$EGFR^{L858R/T790M/C797S}$ kinases activity with an IC_{50} of 71.9 ± 20.9 nm, and inhibited the $EGFR^{L858R/T790M}$ activity with an IC_{50} of 155.2 ± 46.4 nM $EGFR^{C797S}$ mutation was the main cause of acquired resistance to third-generation EGFR TKIs (Chabon et al., 2016). The selectivity of $EGFR^{L858R/T790M/C797S}$ suggested that XHL11 might be a novel $EGFR^{T790M}$ mutant inhibitor with $EGFR^{C797S}$ inhibitory activity, which might overcome the acquired resistance caused by $EGFR^{T790M}$ mutant.

The activation of EGFR was evaluated by Western blotting analysis using H1975 cells with $EGFR^{T790M}$. As shown in Fig. 2, XHL11 inhibited the phosphorylation of EGFR in a dose- and time-dependent manner with no impact on the total EGFR expression.

3.3. XHL11 inhibited proliferation of EGFR-mutant cell lines

To compare the anti-proliferative activity of XHL11 with the other EGFR TKIs, cytotoxic effect of XHL11 on EGFR-mutant cells was determined using MTT assay. As shown in Fig. 3A, XHL11 inhibited the proliferation of H1975 ($EGFR^{T790M}$ positive cells) in a dose and time dependent manner. Moreover, XHL11 inhibited the growth of EGFR-mutant cell lines more potently than AZD9291 and Gefitinib with an incubation of 24 h. Moreover, the antiproliferative activity of XHL11 strengthened with the passage of time, and could dramatically inhibit cell viability at extremely low concentration (1 nM). The anti-proliferative activity of XHL11 on A431 cells was also detected using MTT assay. It turned out that XHL11 inhibited the proliferation of A431 cells more potently than AZD9291 and Gefitinib. In addition, XHL11 exhibited relatively low inhibitory activity on A431 cells than that on H1975 cells following a 72 h drug exposure.

Colony formation assay was performed to further demonstrate the anticancer activity of XHL11. In accordance with the MTT assay, XHL11 inhibited the density and size of the colony formed by H1975 and A431 cells as shown in Fig. 3B. These results revealed that XHL11 inhibited proliferation of EGFR-mutant cell lines. Moreover, XHL11 could also inhibit the proliferation of cell line having EGFR-sensitive mutation. As shown in supplementary Fig. 2, XHL11 inhibited the proliferation of PC9 in a dose and time dependent manner, and inhibited the density and size of the colony formed by PC9 cells.

3.4. XHL11 induced apoptosis in EGFR-mutant cell lines

Annexin V-FITC/propidium iodide (PI) apoptosis analysis was used to investigate the effect of XHL11 on the apoptosis of EGFR-mutant cell lines. As shown in Fig. 4, XHL11 was found to induce apoptosis in both H1975 and A431 cells. The early apoptosis rate induced by XHL11 was 31.0% and 29.1% at the concentration of 0.1 μM and 1 μM in H1975 cells. For the A431 cells, the early apoptosis rate was 31.4% and 36.9% with the similar effect in H1975 cells. While, the late apoptosis rate induced by XHL11 in H1975 was 9.9% (0.1 μM) and 8.0% (1 μM). In contrast, the late apoptosis rate induced by XHL11 in A431 was 31.4% (0.1 μM) and 36.9% (1 μM). These results revealed that XHL11 induced apoptosis in EGFR-mutant cell lines. Gefitinib and AZD9291 exhibited little effect on the apoptosis of H1975 and A431 cells at the concentration of 1 μM.

3.5. XHL11 regulated the apoptosis and EGFR signaling

To confirm the effect of XHL11 on the induction of apoptosis in EGFR-mutant cell lines, the cleavage of PARP and the activation of caspase-3 were detected by Western blotting analysis. In accordance

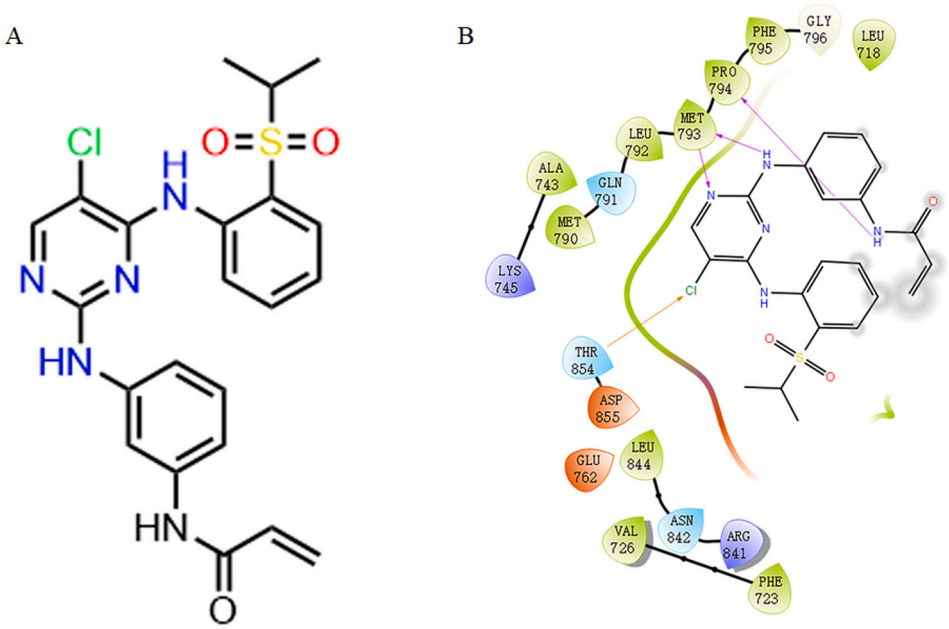

Fig. 1. XHL11 inhibits EGFR kinase activity. (A) Structure and EGFR kinase inhibitory activity of XHL11 (B) The proposed binding mode of compound XHL11 and EGFR. XHL11 interactions with amino acid. XHL11 with carbon atoms colored black, oxygen atoms colored red, nitrogen atoms colored blue, chloride colored green, sulphur colored yellow. Hydrogen bond colored purple, covalent bond colored dark yellow.

Table 2
The effect of XHL11 on the tyrosine kinases activity of wild-type and mutated EGFR.

IC_{50}(nM)	$EGFR^{WT}$	$EGFR^{L858R/T790M}$	$EGFR^{L858R/T790M/C797S}$
XHL11	352.4 ± 90.1	155.2 ± 46.4	71.9 ± 20.9
AZD9291	222.1 ± 99.5	3.1 ± 1.1	nd

nd means no results due to no inhibition.

with the Annexin V-FITC/propidium iodide (PI) apoptosis analysis, PARP and caspase-3 activation was up-regulated by XHL11 in H1975 cells (shown in Fig. 5). Furthermore, XHL11 also down-regulated the downstream signaling including Bcl-xL, AKT and ERK in H1975 cells in a dose- and time-dependent manner.

3.6. XHL11 induced reactive oxidative species generation in EGFR-mutant cell lines

It was reported that AZD9291 induced apoptosis *via* reactive oxygen species generation in non-small cell lung cancer cells (Tang et al., 2017a). Therefore, the levels of reactive oxidative species in H1975 and A431 treated with Gefitinib, AZD9291 and XHL11 was detected. As shown in Fig. 6, reactive oxidative species was increased by XHL11 and AZD9291 in H1975 cells, but not in A431 cells. Gefitinib barely affected

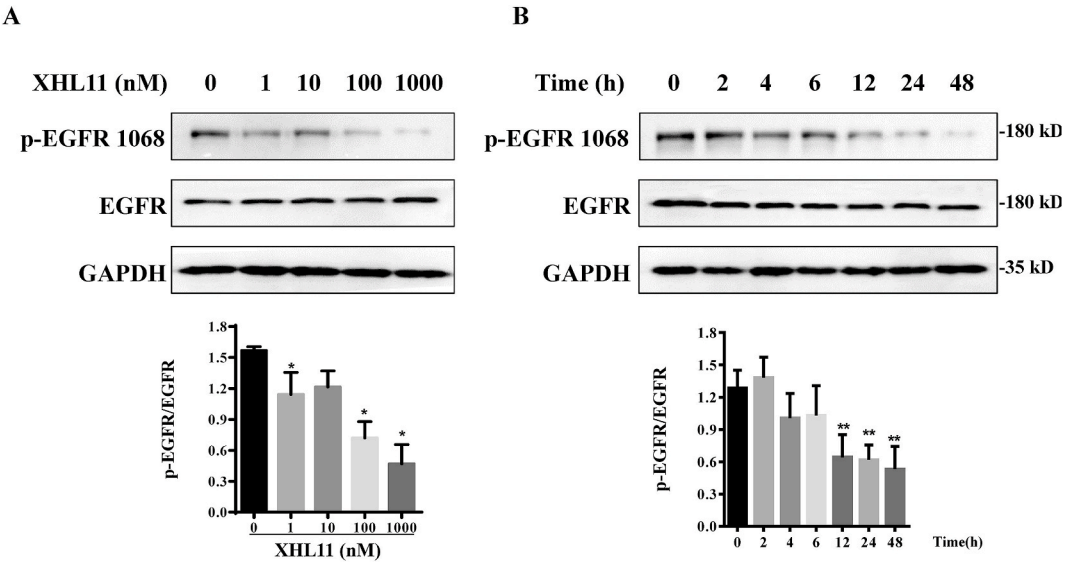

Fig. 2. XHL11 inhibits the activation of EGFR. (A) The expression of P-EGFR and EGFR were assessed by western blot analyses in H1975 cell line after the incubation with XHL11 (1, 10, 100, 1000 nM) for 24 h. (B) The expression of P-EGFR and EGFR were assessed by western blot in H1975 cell line after the incubation with XHL11 (0.1 μM) for 2, 4, 6, 12, 24 h. Data were represented as mean ± S.D. of triplicate determinations. *P < 0.05, **P < 0.01, significantly different compared with the DMSO-treated control by one-way ANOVA followed by Dunnett's test.

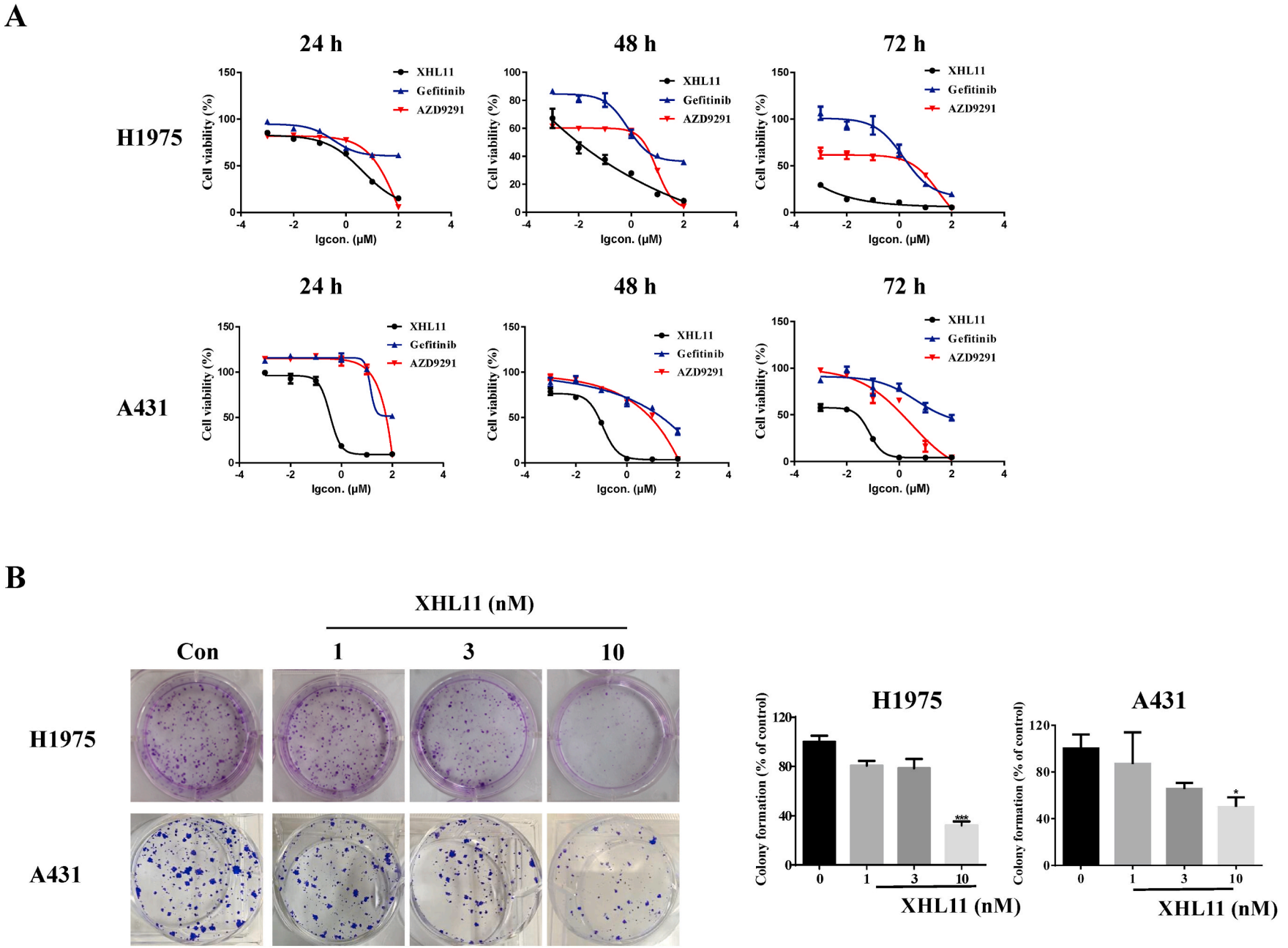

Fig. 3. Effects of XHL11 on the proliferation of EGFR-mutant cell lines. (A) Effects of XHL11 on cell viability of EGFR-mutant cell lines. H1975 and A431 cells were incubated with increasing concentrations of XHL11 (from 0.001 to 100 μM) for 24, 48, 72 h. Cell viability was detected by MTT assay. The percentage of cell viability was calculated by the absorption of control cells (0.1% DMSO) as 100%. (B) Effects of XHL11 on the colony forming ability of EGFR-mutant cell lines. Cells were incubated with XHL11 (1, 3, 10 nM) for 48 h, and then cultured with fresh media for 10 d. Data were represented as mean ± S.D. of triplicate independent studies. *P < 0.05, significantly different compared with the DMSO-treated control by one-way ANOVA followed by Dunnett's test.

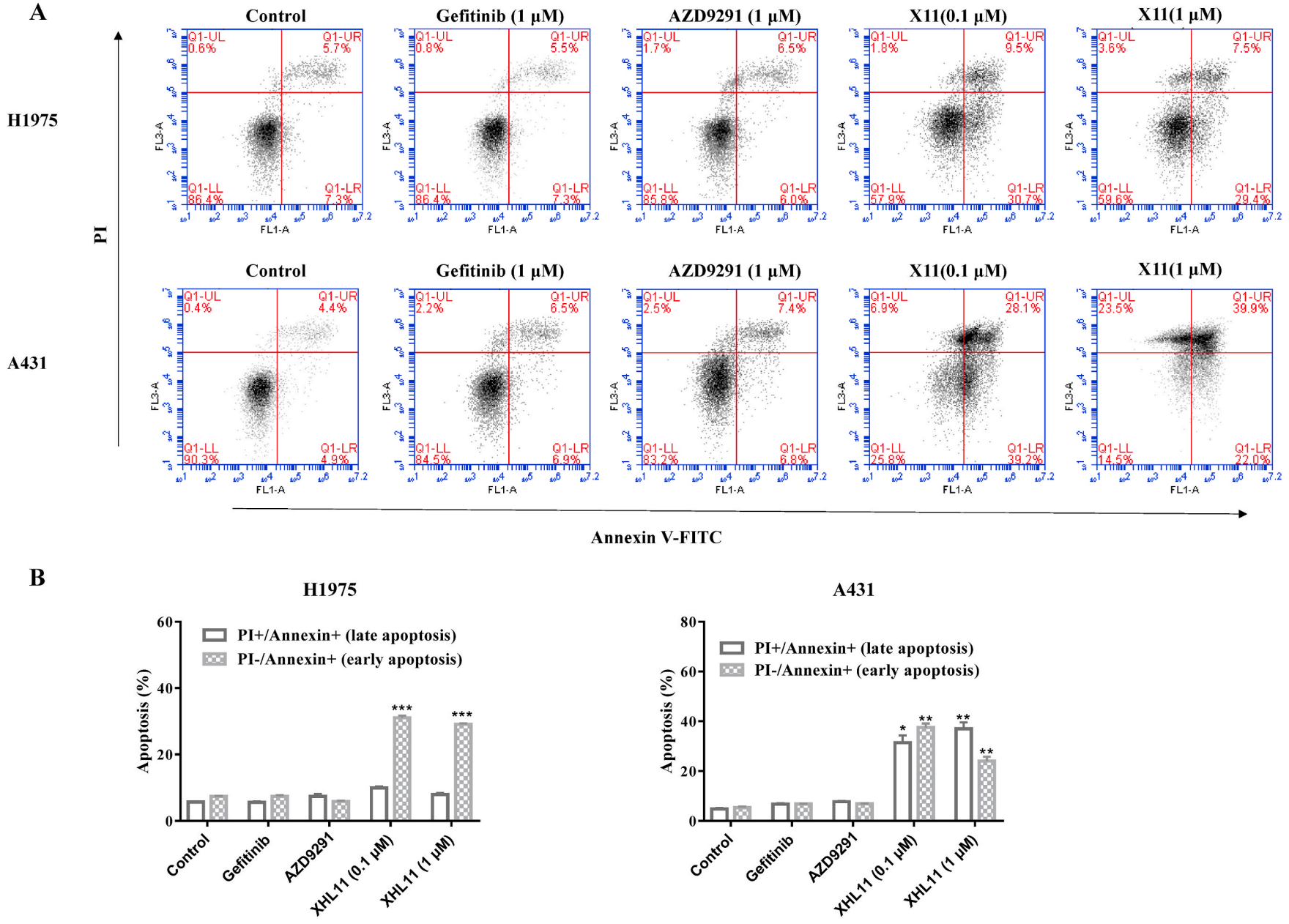

Fig. 4. XHL11 induced apoptosis in EGFR-mutant cell lines. (A) Cells were incubated with Gefitinib (1 μM), AZD9291 (1 μM), XHL11 (0.1 and 1 μM) for 24 h, and stained by Annexin V staining and propidium iodide (PI). (B) The percentage of PI+/Annexin + cells (late apoptosis) and PI-/Annexin + cells (early apoptosis). Data were represented as mean ± S.D. of triplicate independent determinations. *P < 0.05, ***P < 0.001, significantly different compared with the DMSO-treated control by one-way ANOVA followed by Dunnett's test.

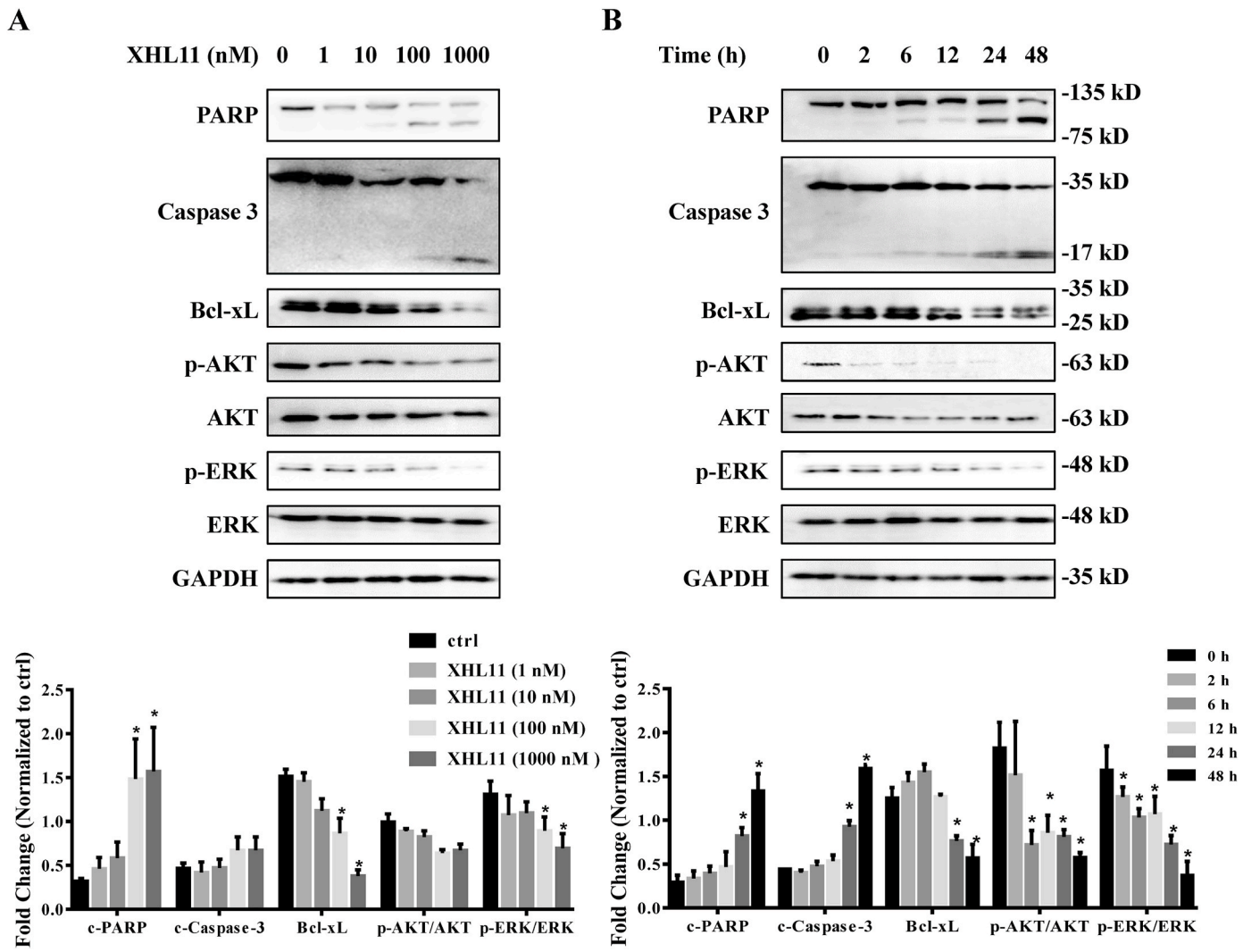

Fig. 5. XHL11 induces apoptosis and regulates apoptosis-related protein and EGFR signaling in a dose and time dependent manner. (A) H1975 cells were assessed by western blot analyses after the incubation with XHL11 (1, 10, 100, 1000 nM) for 24 h. (B) The cleavage of PARP, Caspase 3, and the expression of Bcl-xL, P-AKT and P-ERK were assessed by western blot in H1975 cell line after the incubation with XHL11 (0.1 μM) for 2, 6, 12, 24 h. Data were represented as mean ± S.D. of triplicate independent studies. *P < 0.05, significantly different compared with the DMSO-treated control by one-way ANOVA followed by Dunnett's test.

reactive oxidative species generation in both cells. To confirm the role of reactive oxidative species generation on the apoptosis induction of XHL11, the H1975 cells were pretreated with NAC, which is known as an inhibitor of reactive oxidative species, and then incubated with XHL11 for 24 h. The pretreating of NAC (5 mM) not only reduced the production of reactive oxidative species induced by XHL11 but also counteract the effect of XHL11 on apoptosis. Therefore, we conjectured that reactive oxidative species played an important role in the anticancer effect and apoptosis induction of XHL11.

3.7. XHL11 inhibited tumor growth in the H1975 subcutaneous xenograft model in vivo

To further investigate the anti-tumor effect of XHL11 *in vivo*, a H1975 subcutaneous xenograft model was established in BALB/c nude mice. The mice were intragastric administrated with XHL11 (60 mg/kg) twice a week *via* oral gavage for 17 days. As shown in Fig. 7, XHL11 inhibited tumor growth in the H1975 subcutaneous xenograft mice without significant changes in body weight. To confirm the anti-proliferation capability, we also investigated the expression of Ki67, P-EGFR, EGFR by immunohistochemical analysis. As shown in Fig. 7C–D, XHL11 inhibited the EGFR phosphorylation and down-regulated the expression of Ki-67 which indicated that XHL11 suppressed tumor cell proliferation. Moreover, TUNEL staining of the tumor tissue showed that XHL11 induced apoptosis *in vivo*.

4. Discussion

Lung cancer is the most commonly diagnosed cancer (11.6% of the total cases) and also the leading cause of cancerous mortality throughout the world (18.4% of the total cancer deaths) with poor prognosis (Bray et al., 2020). Remarkable achievement has been recognized in the treatment of lung cancer over the past few years, among which EGFR targeted therapy is the most prominent. Gefitinib as a representative of the first generation reversible EGFR TKIs, is the standard first-line drug for treatment of EGFR-mutant lung cancer. However, the acquired resistance caused by the mutation of $EGFR^{T790M}$ spawned the third generation EGFR TKIs, such as AZD9291, which was approved by the FDA as a second-line treatment for lung cancer with resistance caused by $EGFR^{T790M}$ mutant. Despite the high efficacy, AZD9291 was reported to acquire resistance with $EGFR^{C797S}$ mutation (Kim et al., 2015), which was the most common mechanism of AZD9291 resistance. Besides, the high price and adverse reaction limited the prescription of the drug. Therefore, more effort should be devoted to develop novel

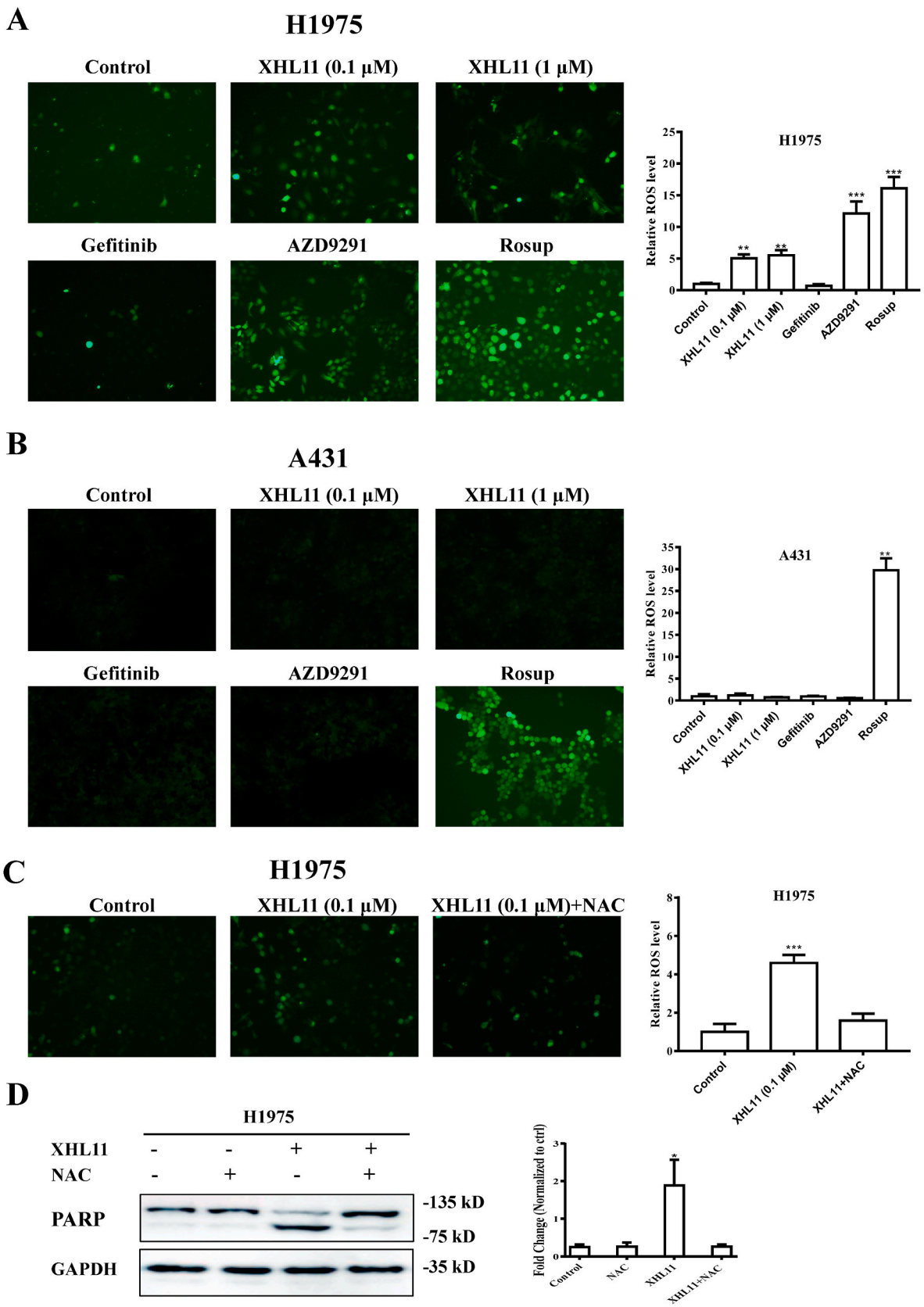

Fig. 6. XHL11 induces ROS generation in EGFR-mutant cell lines. (A–B) Cells were treated with Gefitinib (1 μM), AZD9291 (1 μM), XHL11 (0.1 and 1 μM) for 24 h, and the Rosup compound mixture for 30 min, and labelled with DCFH-DA (10 μM) for 1 h before the detection. (C) H1975 cells were pretreated with NAC (5 mM) and then incubated with XHL11 for 24 h, and labelled with DCFH-DA (10 μM) for 1 h before the detection. (D) The apoptosis was measured by the cleavage of PARP. The photographs were taken at magnifications of × 200. Data were expressed as % of control and were represented as mean ± S.D. of triplicate independent studies. *P < 0.05, **P < 0.01, ***P < 0.001, significantly different compared with the control group.

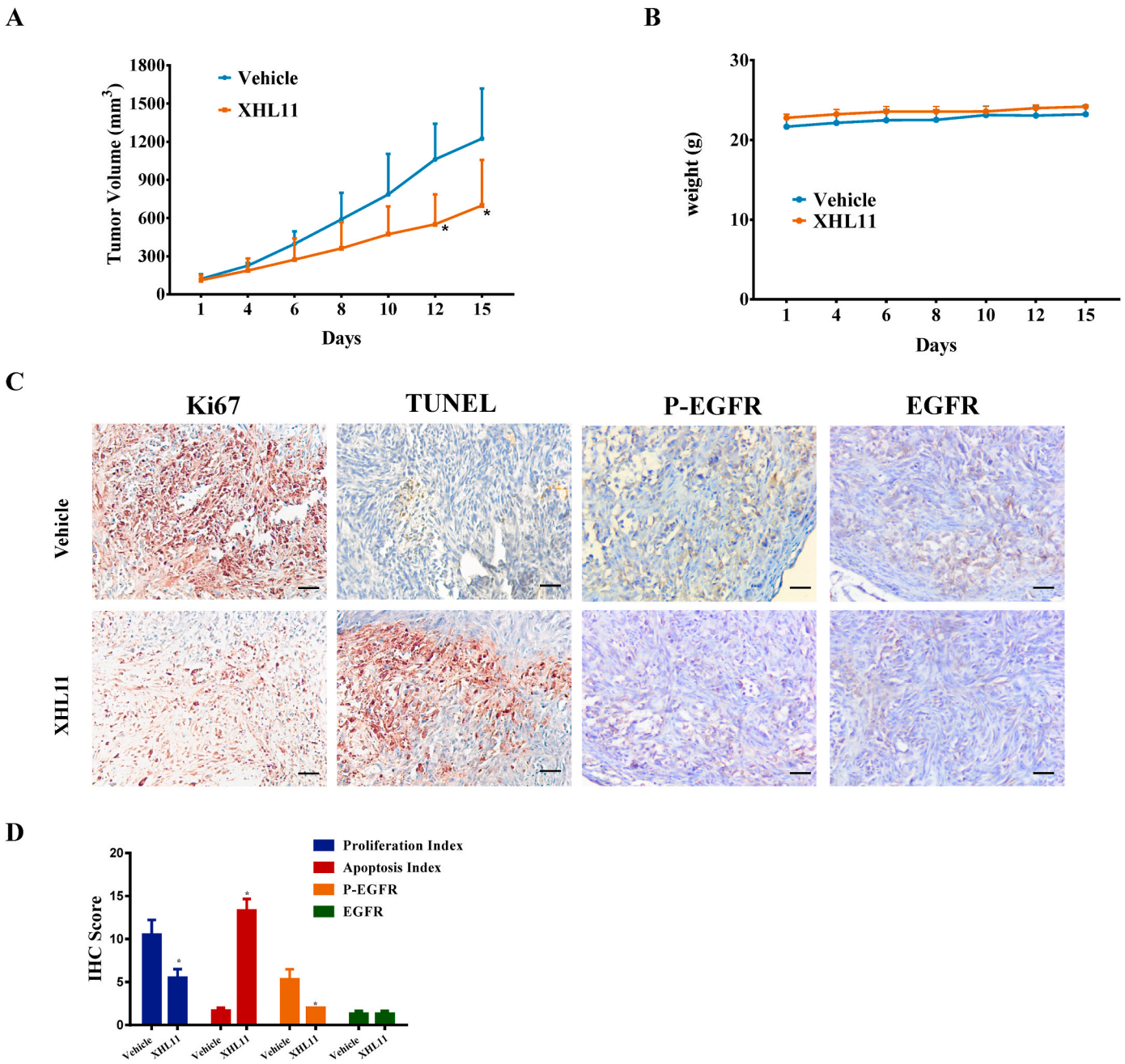

Fig. 7. XHL11 inhibited tumor growth in the H1975 subcutaneous xenograft model. (A) The mice were orally administrated with vehicle, XHL11 (60 mg/kg) twice a week for 17 days. Tumor volumes measured three times a week are expressed as mean values ± S.D. (n = 5). *P < 0.05, significantly different compared with control group. (B) The body weight expressed as mean values ± S.D. (C) Representative photographs of tumor tissues stained with Ki67, P-EGFR, EGFR and TUNEL staining of the tumor tissue. The photographs were taken at magnifications of × 200. Scale bar, 50 μm. (D) Quantification of Ki67 (proliferation index), apoptosis index assessed by TUNEL, P-EGFR and EGFR. Data were represented as mean ± S.D. of triplicate independent studies. *P < 0.05, significantly different compared with control group.

mutant-selective EGFR TKIs. Alternative drugs should be developed to cut the costs and mitigate the side effects.

In this study, we aim to investigate whether XHL11 could inhibit the growth of **EGFR^{T790M}**-mutant NSCLC cells. It turned out that XHL11 inhibited the proliferation of H1975 cells more efficiently than AZD9291, and induced apoptosis in EGFR mutant cell lines at the concentration 0.1 μM. While, AZD9291 couldn't induce apoptosis of H1975 and A431 cells at the concentration of 1 μM. In this study, XHL11 was demonstrated to inhibit the EGFR$^{L858R/T790M}$ and EGFR$^{L858R/T790M/C797S}$ kinases activity. It indicated the potential that XHL11 might overcome EGFR^{C797S} mutation. However, this research was focused on the effect of XHL11 against the secondary (T790M) EGFR mutations. Further study is underway to find out the effect of XHL11 using an EGFR$^{L858R/T790M/C797S}$ cell line. Moreover, XHL11 inhibited the phosphorylation of EGFR and downstream pathways including Bcl-xL, AKT and ERK in a dose- and time-dependent manner. Furthermore, XHL11 suppressed tumor volume in the H1975 subcutaneous xenograft mice without significant changes in body weight. In accordance with the *in vitro* results, XHL11 inhibited the EGFR phosphorylation and the expression of Ki-67. Moreover, XHL11 was detected to induce apoptosis *in vivo* by TUNEL staining. These results demonstrated that XHL11 exhibited high antitumor activity and could be developed as a promising EGFR TKI.

There is a wide spread agreement that elevated reactive oxidative species is one of the hallmarks of cancer cells. Contradictory evidence has emerged during the research of reactive oxidative species. On the one hand, cancer cells stimulated reactive oxidative species to facilitate proliferation and accelerate the tumor progression. Reactive oxidative species assists the cancer cells to maintain malignant phenotypes and plays an important part in regulating the proliferation, differentiation, and apoptosis in cancer cells [18]. On the other hand, oxidant stress induced intracellular reactive oxidative species level to a toxicity concentration, which could be exploited in the development of a therapeutic agent and could selectively kill cancer cells (Lampiasi et al., 2009). The elevated level of reactive oxidative species devoted to the intracellular dysfunction through damaging to DNA, arresting cell cycle and inducing apoptosis. To sum up, tumor cells may die by the same sword they benefit from (Zhang et al., 2021). In accordance with the previous reports (Hu et al., 2020; Tang et al., 2017b), AZD9291 induced the generation of H_2O_2 in H1975 cells. In the present study, XHL11 was also found to promote reactive oxidative species generation in H1975 but in A431 cell line. It's possible that H_2O_2 was not elicited in A431 because of the cell type, the culture environment, the concentration and the incubation time. Moreover, XHL11 was found to induce apoptosis of cancer cells through the regulation of the EGFR pathway involving AKT and ERK. Further study is underway to determine whether XHL11 promote reactive oxidative species generation through the inhibition of EGFR.

In conclusion, this research evaluated XHL11 as a novel EGFR inhibitor which markedly inhibited the proliferation, induced apoptosis of $EGFR^{T790M}$-mutant NSCLC cells. Moreover, the down-regulation of EGFR and down-stream signaling devoted to the apoptosis and the anti-proliferation of XHL11. This study demonstrated XHL11 might serve as a novel promising EGFR TKI for the treatment of NSCLC patients.

Authors contributions

Yi Li, Hong-Lei Xie, and Chun-Guang Ren designed the research. All the authors performed *in vitro* and *in vivo* experiments. Yi Li and Qinglong Yu performed data analysis and wrote the manuscript.

Data availability statement

The data that support the findings of this study are available from the corresponding author upon reasonable request.

CRediT authorship contribution statement

Yi Li: Formal analysis, Writing – original draft, designed the research, carried out the experiment and statistical analysis, and wrote the manuscript. **Qing-Long Yu:** Formal analysis, carried out the experiment and statistical analysis. **Tong-Fang Li:** carried out the experiment, All of the authors have read and approved the fnal manuscript. **Ya-Ni Xiao:** carried out the experiment, All of the authors have read and approved the fnal manuscript. **Li Zhang:** carried out the experiment, All of the authors have read and approved the fnal manuscript. **Qiu-Yan Zhang:** designed the research and edited the manuscript. **Chun-Guang Ren:** designed the research and edited the manuscript. **Hong-Lei Xie:** designed the research and edited the manuscript.

Declaration of competing interest

There is no conflict of interest declared by the authors.

Acknowledgements

The authors gratefully appreciate the financial support from Shandong Provincial Natural Science Foundation, China (ZR2019BH087, ZR2020QH256, 2019GSF108050), and Yantai Science and Technology Bureau, China (2019MSGY128).

Appendix A. Supplementary data

Supplementary data to this article can be found online at https://doi.org/10.1016/j.ejphar.2021.174297.

References

Bray, F., Ferlay, J., Soerjomataram, I., Siegel, R.L., Torre, L.A., Jemal, A., 2018. Global cancer statistics 2018: GLOBOCAN estimates of incidence and mortality worldwide for 36 cancers in 185 countries. Ca-Cancer J Clin. 68, 394–424.

Bray, F., Ferlay, J., Soerjomataram, I., Siegel, R.L., Torre, L.A., Jemal, A., 2020. pg 394, 2018. In: Global Cancer Statistics 2018: GLOBOCAN Estimates of Incidence and Mortality Worldwide for 36 Cancers in 185 Countries, vol. 68. Ca-Cancer J Clin.

Camidge, D.R., Pao, W., Sequist, L.V., 2014. Acquired resistance to TKIs in solid tumours: learning from lung cancer. Nat. Rev. Clin. Oncol. 11, 473–481.

Chabon, J.J., Simmons, A.D., Lovejoy, A.F., Esfahani, M.S., Newman, A.M., Haringsma, H.J., et al., 2016. Circulating tumour DNA profiling reveals heterogeneity of EGFR inhibitor resistance mechanisms in lung cancer patients. Nat. Commun. 7, 11815.

Engelman, J.A., Janne, P.A., 2008. Mechanisms of acquired resistance to epidermal growth factor receptor tyrosine kinase inhibitors in non-small cell lung cancer. Clin. Canc. Res. 14, 2895–2899.

Goss, G., Tsai, C.M., Shepherd, F.A., Bazhenova, L., Lee, J.S., Chang, G.C., et al., 2016. Osimertinib for pretreated EGFR Thr790Met-positive advanced non-small-cell lung cancer (AURA2): a multicentre, open-label, single-arm, phase 2 study. Lancet Oncol. 17, 1643–1652.

Hao, Y.J., Wang, X., Zhang, T., Sun, D.H., Tong, Y., Xu, Y.Q., et al., 2016. Discovery and structural optimization of N5-substituted 6,7-Dioxo-6,7-dihydropteridines as potent and selective epidermal growth factor receptor (EGFR) inhibitors against L858R/T790M resistance mutation. J. Med. Chem. 59, 7111–7124.

Heigener, D.F., Reck, M., 2011. Mutations in the epidermal growth factor receptor gene in non-small cell lung cancer: impact on treatment beyond gefitinib and erlotinib. Adv. Ther. 28, 126–133.

Hu, X., Zhang, Z.Y., Wu, L.W., Zeng, L.H., Chen, H., Zhu, H.J., et al., 2020. A natural anthraquinone derivative shikonin synergizes with AZD9291 against wtEGFR NSCLC cells through reactive oxygen species-mediated endoplasmic reticulum stress. Phytomedicine 68.

Janne, P.A., Yang, J.C.H., Kim, D.W., Planchard, D., Ohe, Y., Ramalingam, S.S., et al., 2015. AZD9291 in EGFR inhibitor-resistant non-small-cell lung cancer. N. Engl. J. Med. 372, 1689–1699.

Kim, T.M., Song, A., Kim, D.W., Kim, S., Ahn, Y.O., Keam, B., et al., 2015. Mechanisms of acquired resistance to AZD9291 A mutation-selective, irreversible EGFR inhibitor. J. Thorac. Oncol. 10, 1736–1744.

Kobayashi, S., Boggon, T.J., Dayaram, T., Janne, P.A., Kocher, O., Meyerson, M., et al., 2005. EGFR mutation and resistance of non-small-cell lung cancer to gefitinib. N. Engl. J. Med. 352, 786–792.

Ku, B.M., Bae, Y.H., Koh, J., Sun, J.M., Lee, S.H., Ahn, J.S., et al., 2016. AZD9291 overcomes T790 M-mediated resistance through degradation of EGFR(L858R/T790M) in non-small cell lung cancer cells. Invest. N. Drugs 34, 407–415.

Lampiasi, N., Azzolina, A., D'Alessandro, N., Umezawa, K., McCubrey, J.A., Montalto, G., et al., 2009. Antitumor effects of dehydroxymethylepoxyquinomicin, a novel nuclear factor-kappa B inhibitor, in human liver cancer cells are mediated through a reactive oxygen species-dependent mechanism. Mol. Pharmacol. 76, 290–300.

Murtuza, A., Bulbul, A., Shen, J.P., Keshavarzian, P., Woodward, B.D., Lopez-Diaz, F.J., et al., 2019. Novel third-generation EGFR tyrosine kinase inhibitors and strategies to overcome therapeutic resistance in lung cancer. Canc. Res. 79, 689–698.

Niederst, M.J., Hu, H.C., Mulvey, H.E., Lockerman, E.L., Garcia, A.R., Piotrowska, Z., et al., 2015. The allelic context of the C797S mutation acquired upon treatment with third-generation EGFR inhibitors impacts sensitivity to subsequent treatment strategies. Clin. Canc. Res. 21, 3924–3933.

Ortiz-Cuaran, S., Scheffler, M., Plenker, D., Dahmen, L., Scheel, A.H., Fernandez-Cuesta, L., et al., 2016. Heterogeneous mechanisms of primary and acquired resistance to third-generation EGFR inhibitors. Clin. Canc. Res. 22, 4837–4847.

Pao, W., Miller, V.A., Politi, K.A., Riely, G.J., Somwar, R., Zakowski, M.F., et al., 2005. Acquired resistance of lung adenocarcinomas to gefitinib or erlotinib is associated with a second mutation in the EGFR kinase domain. PLoS Med. 2, 225–235.

Park, K., Tan, E.H., O'Byrne, K., Zhang, L., Boyer, M., Mok, T., et al., 2016. Afatinib versus gefitinib as first-line treatment of patients with EGFR mutation-positive non-small-cell lung cancer (LUX-Lung 7): a phase 2B, open-label, randomised controlled trial. Lancet Oncol. 17, 577–589.

Rosell, R., Moran, T., Queralt, C., Porta, R., Cardenal, F., Camps, C., et al., 2009. Screening for epidermal growth factor receptor mutations in lung cancer. N. Engl. J. Med. 361, U938–U958.

Sequist, L.V., Yang, J.C.H., Yamamoto, N., O'Byrne, K., Hirsh, V., Mok, T., et al., 2013. Phase III study of afatinib or cisplatin plus pemetrexed in patients with metastatic lung adenocarcinoma with EGFR mutations. J. Clin. Oncol. 31, 3327.

Tan, C.S., Cho, B.C., Soo, R.A., 2016. Next-generation epidermal growth factor receptor tyrosine kinase inhibitors in epidermal growth factor receptor -mutant non-small cell lung cancer. Lung Canc. 93, 59–68.

Tang, Z.H., Cao, W.X., Su, M.X., Chen, X., Lu, J.J., 2017a. Osimertinib induces autophagy and apoptosis via reactive oxygen species generation in non-small cell lung cancer cells. Toxicol. Appl. Pharmacol. 321, 18–26.

Tang, Z.H., Cao, W.X., Su, M.X., Chen, X.P., Lu, J.J., 2017b. Osimertinib induces autophagy and apoptosis via reactive oxygen species generation in non-small cell lung cancer cells. Toxicol. Appl. Pharmacol. 321, 18–26.

Thress, K.S., Paweletz, C.P., Felip, E., Cho, B.C., Stetsonl, D., Dougherty, B., et al., 2015. Acquired EGFR C797S mutation mediates resistance to AZD9291 in non-small cell lung cancer harboring EGFR T790M. Nat. Med. 21, 560–562.

Walter, A.O., Sjin, R.T.T., Haringsma, H.J., Ohashi, K., Sun, J., Lee, K., et al., 2013. Discovery of a mutant-selective covalent inhibitor of EGFR that overcomes T790M-mediated resistance in NSCLC. Canc. Discov. 3, 1404–1415.

Yu, H.A., Schoenfeld, A.J., Makhnin, A., Kim, R., Rizvi, H., Tsui, D., et al., 2020. Effect of osimertinib and bevacizumab on progression-free survival for patients with metastatic EGFR-mutant lung cancers: a phase 1/2 single-group open-label trial. JAMA Oncol 6, 1048–1054.

Zhang, J., Duan, D., Song, Z., Liu, T., Hou, Y., Fang, J., 2021. Small molecules regulating reactive oxygen species homeostasis for cancer therapy. Med. Res. Rev. 41, 342–394.

Zhou, W.J., Ercan, D., Chen, L., Yun, C.H., Li, D.N., Capelletti, M., et al., 2009. Novel mutant-selective EGFR kinase inhibitors against EGFR T790M. Nature 462, 1070–1074.